

## Hollow-Polyaniline-Sphere-Coated Sensor For Measuring Gas-Phase OH Radicals According To The Change In Electrical Conductivity

Bao Lin\*, Shu-Liang Liaw\*\*

\*(Graduate Institute of Environmental Engineering, National Central University, 300 Zhongda Road, Zhongli, Taoyuan, Taiwan

\*\* (Graduate Institute of Environmental Engineering, National Central University, 300 Zhongda Road, Zhongli, Taoyuan, Taiwan

### ABSTRACT

In advanced oxidation processes, OH radicals play a crucial role in enhancing the removal efficiency of volatile organic compounds. In this paper, hollow polyaniline (PANI) spheres were coated onto a conducting ceramic honeycomb substrate to form a PANI sensor for detecting the concentration of OH radicals in the amorphous phase. The hollow PANI spheres were effectively synthesized through a double-surfactant-layer-assisted polymerization process by using  $\text{Fe}_3\text{O}_4$  nanoparticle as the core template. The PANI shell thickness, morphology characterizations and specific surface area were controlled by altering the weight of aniline monomers. The electrical conductivity served as a function of the operating temperature and specific surface area, which is a characteristic behavior of conductive polymer materials in the atmosphere. At an optimized temperature of  $125^\circ\text{C}$  and specific surface area of  $1435 \text{ m}^2/\text{g}$ , the PANI sensor reacted with a high amount of OH radicals generated from the decomposition of ozone over  $\alpha\text{-FeOOH}$  nanoparticles. The conductometric response after the OH radical attack increased exponentially with the concentration of the OH radicals.

**Keywords:-** electrical conductivity, OH radical, polyaniline

### I. INTRODUCTION

Volatile organic compounds (VOCs) deteriorate indoor air quality and human health. Advanced oxidation processes including transition metal oxide catalytic ozonation and photocatalysis can adequately remove gas-phase VOCs [1-3]. In these advanced oxidation processes, OH radicals play a crucial role in enhancing the VOC removal efficiency [4,5]. Measuring gas-phase OH radicals is extremely difficult because of their high reactivity and short lifetime (less than  $10^{-9}$  s) [6]. Technologies such as laser-induced fluorescence, ultraviolet-visible optical emission spectroscopy, and high-performance liquid chromatography (HPLC) coupled with electrochemical detection facilitate adequately measuring OH radicals [7-9]. However, operating these technologies is expensive and complex. Therefore, developing easy-to-use, cost-effective, and highly sensitive electronic sensors for detecting OH radicals is imperative.

Conducting polymers (CPs), such as polyaniline (PANI), polyacetylene, polypyrrole, and polythiophene, have recently attracted considerable research attention because of their metallic conductivity [10-12]. The charge defects of CPs can be formed through chemically or electrochemically induced oxidation [13]. Therefore, CPs can scavenge for reactive oxygen species in the liquid phase [14-16]. Among the various CPs, PANI has attracted

considerable attention because of its superior electrical conductivity and chemical stability. In this study, we developed hollow PANI spheres and coated them on a conducting porous ceramic substrate to form a sensor (PANI sensor) for detecting OH radicals. Target gas was pumped onto the surface of the PANI sensor. The concentration of OH radicals can be determined by detecting the conductometric behavior of the PANI sensor.

In situ polymerization of aniline in the presence of nanoparticles has been frequently used for preparing hollow polymer spheres [17,18]. The preparation process is described in Fig. 1. The PANI shell was coated on the surface of the core template through a polymerization reaction in a solution phase. When a homogeneous PANI shell was formed uniformly and completely on the core template, the hollow PANI sphere was obtained by etching the template core.

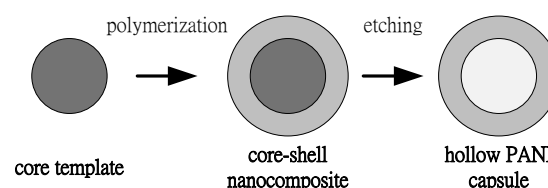


**Fig. 1:** Synthesis scheme for a monodisperse hollow PANI sphere

The main disadvantage of this approach is that controlling the thickness of the derived PANI sphere is difficult. Nanosized particles in aqueous solution are easily agglomerated [19], and because of this agglomeration, the rate of polymerization on the surface of the core cannot remain lower than that in the solution [20]. External forces such as ultrasound effects can break the nanoparticle agglomerates into smaller agglomerates; however, the process is complex and expensive to operate [21]. In addition, PANI is an organic semiconductor with thermally activated conduction mechanisms.

In this study, Fe<sub>3</sub>O<sub>4</sub> nanoparticles were used as the core template, and hollow PANI spheres were synthesized through a double-surfactant-layer-assisted polymerization process [22,23]. The shell thickness was controlled by modulating the weight of aniline monomers, and the operating-temperature-dependent conductivity was considered a function of shell thickness. At an optimized operating temperature and shell thickness, the conductometric behavior of the OH radical attacks was analyzed. The OH radicals were generated through ozone decomposition over  $\alpha$ -FeOOH nanoparticles. The formed OH radicals were determined using the hydroxylation of salicylic acid (SAL) [24] caused from the catalytic ozonation.

## II. Experimental and Methods

### 2.1 Preparation of the Fe<sub>3</sub>O<sub>4</sub> Core

Fe<sub>3</sub>O<sub>4</sub> nanoparticles (mean crystallite size = 30  $\mu$ m) served as the catalyst core. The selected Fe<sub>3</sub>O<sub>4</sub> nanoparticles (100 g) were dispersed in deionized water (500 mL), and polyethylene glycol (PEG; 100 g) was added to this dispersion and then constantly stirred for 24 h. After the stirring was completed, the nanoparticles were washed repeatedly with dilute acetone until the unabsorbed PEG molecules were completely removed. Subsequently, the PEG-absorbed Fe<sub>3</sub>O<sub>4</sub> nanoparticles were dried at 60°C for another 24 h.

### 2.2 Synthesis of the Core-Shell Nanocomposites

The required amount of aniline monomer (Merck Company, Germany) was distilled for 60 min under vacuum and stored at 5 °C before use. The PEG-absorbed Fe<sub>3</sub>O<sub>4</sub> nanoparticles (100 g), dodecyl benzene sulfonic acid (DBSA; 20 g), potassium persulfate (20 g) and 1000 mL pure water were thoroughly mixed using to obtain a uniform suspension. The aniline monomer and 500 mL of HCl solution (20 mM) were subsequently added to the derived suspension. The mixture was slowly stirred at room temperature for 24 h for polymerization. After the polymerization process was completed, the sample solution in the sample holder was cooled and completely frozen at -40°C. The obtained frozen samples were subsequently freeze-dried for 48 h in a vacuum chamber. In order

to obtain the hollow PANI spheres, the resulting Fe<sub>3</sub>O<sub>4</sub> (core)-PANI(shell) products (FP products) were immersed in 1.0 M HCl for 24 h. Hollow PANI capsules were obtained from the FP products by using 1 wt % HF to etch the silica layer and 1.0 M HCl to etch the Fe<sub>3</sub>O<sub>4</sub> core [25]. The obtained PANI capsules were coated on a 200-g conducting Si<sub>3</sub>N<sub>4</sub>/Si ceramic honeycomb substrate (with a 5-cm diameter). Two electrodes composed of 200 Å Ag layers were deposited onto the substrate through plasma-enhanced chemical vapor deposition [26]. The amounts of aniline used in the experiments were 50, 100, 150, 200, 250, and 300 g.

### 2.3. Detection of OH Radicals

Before the tests, a  $\alpha$ -FeOOH catalytic filter was fabricated as follows. Under a vacuum, the as-prepared  $\alpha$ -FeOOH nanoparticles (20 g) were coated onto the surface of a 200-g ceramic honeycomb substrate (with a 5-cm diameter). The coating steps followed those described in US Patent No. 7,521,087 [27]. When the tests were started, clean air acted as a carrier gas, conveying ozone gas and then into the FP sensor and the  $\alpha$ -FeOOH catalytic filter simultaneously for the OH radical measurements. The electrodes of the PANI sensor were connected to Keithely 2100 electrometer to monitor the DC conductivity. The ozone generator produced ozone gas with a maximal output of 0.1 L/min at 100 ppm. The experiments were conducted at a constant voltage (220 V). Table 1 lists the operating conditions used in the experiments.

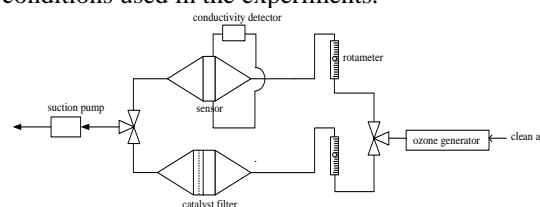


**Fig. 2:** Schematic of the experimental setup for detecting the OH radicals

**TABLE 1:** Experimental Conditions in the Detection of OH Radicals

Condition	Value
Gas flow rate (L/min)	2.5
Reaction temperature (°C)	25–300
Relative humidity (%)	0–80
Retention time (s)	0.5
Initial concentration of ozone gas (ppm)	1–100
Duration of experiment in each run (min)	60

## III. ANALYSIS

### 3.1 Physical Characterizations of the Samples

The morphology of the samples was observed under a Cam Scan MV 2300 scanning electron microscope (SEM) with an accelerating voltage of 100 kV. X-ray diffraction (XRD) patterns were taken on a

Siemens D5000 X-ray diffractometer with a Cu K $\alpha$  X-ray radiation ( $\lambda=0.154$  nm). Specific surface area measurements of the fresh catalyst were based on the N<sub>2</sub> adsorption–desorption porosimetry at 77 K, and the surface areas were measured using the Brunauer–Emmett–Teller (BET) method (Micromeritics Gemini-2380). The crystalline size was determined using XRD patterns and the Scherrer equation at  $2\theta = 30^\circ$ . The mean pore diameter ( $\bar{d}$  in nm) was determined using the following equation (1) [28]:

$$\bar{d} = (2 \times 10^{-3} e) / (S_{BET}) \quad (1)$$

where the pore volume ( $e$ ) is expressed in cm<sup>3</sup>/g and the BET surface area ( $S_{BET}$ ) is expressed in m<sup>2</sup>/g

### 3.2 Concentration of Ozone

Ozone concentrations were monitored using an ozone ultraviolet photometry analyzer (Seki Electronics SOZ-302C, Japan).

### 3.3 Concentration of OH Radicals

The formed OH radicals were determined through the hydroxylation of salicylic acid (SAL). The OH radicals emitted from the  $\alpha$ -FeOOH catalytic filter were collected on a sheet of filter paper (inner diameter, 200 mm). The paper was dripped equably with a 15-mL solution containing 1.0 g of SAL and anhydrous ethanol (99.9%). The paper was dried and weighed until the entire solution was loaded onto it. Throughout the hydroxylation of SAL by OH radicals at the gas–solid interface, the film collection efficiency approached 100%. Chemicals on the paper were carefully removed using 500 mL of pure water and subjected to characterization. The OH radical concentration was measured by monitoring the concentrations of 2,3-dihydroxybenzoic acid, catechol, and 2,5-dihydroxybenzoic acid resulting from the attack of OH radicals. The presence of 2,3-dihydroxybenzoic acid, catechol, and 2,5-dihydroxybenzoic acid in the DI water was determined using a high-performance liquid chromatography instrument (Waters 600, Japan). The obtained chromatographic parameters were similar to those reported previously [29]. The photocatalytic activity was determined using the OH radical concentration, which was calculated as follows:

$$C_{OH} = \frac{\sum C_i \times V_L \times N}{F_g \times t} \quad (2)$$

where  $C_{OH}$  is the concentration of OH radicals,  $C_i$  is the concentration of hydroxylated derivatives formed during sampling (mol/L),  $V_L$  is the volume of the scrubbing solution after sampling (L),  $N$  is Avogadro's number,  $F_g$  is the air flow rate (mL/min), and  $t$  is the sampling period (min).

### 3.4 Electrical Conductivity of the PANI Sensor

The DC conductivities of the nanocomposites were measured according to a four-probe method by using

a Keithley 2400 meter. Moreover, the DC conductivities of the samples were obtained by measuring the current flowing through a piece of the material and by using the sample dimension  $\sigma$ , which was determined as follows [30]:

$$\sigma = \left( \frac{d}{AV} \right) \times I \quad (3)$$

where  $\sigma$  is the DC conductivity (s/cm),  $d$  (cm) is the sample thickness of the material,  $A$  is the material area (cm<sup>2</sup>),  $V$  is the potential difference across the material, and  $I$  is the current flowing through the material. The conductometric value related to the OH radicals was calculated as follows:

$$\Delta\sigma = \frac{\sigma_1 - \sigma_2}{\sigma_2} \times 100\% \quad (4)$$

where  $\Delta\sigma$  (%) is the conductivity drop in the FP sensor, and  $\sigma_1$  and  $\sigma_2$  are the conductivity values before and after the OH radical attack from the consumption of the required ozone.

## IV. DISCUSSIONS

### 4.1 Physical Properties of the Prepared Samples

Fig. 3 shows the XRD patterns of the FP samples obtained by altering the PF ratio. The patterns corresponded to pure Fe<sub>3</sub>O<sub>4</sub>, and this finding is confirmed by JCPDS Pattern No. 75-0033 [31,32]. The diffraction peaks of Fe<sub>3</sub>O<sub>4</sub> were adequately maintained in the FP samples, and the peak intensity of Fe<sub>3</sub>O<sub>4</sub> decreased as the content of aniline monomer increased in the FP sample. The performance indicates that the crystallite size of Fe<sub>3</sub>O<sub>4</sub> remained unchanged during the polymerization process. A broad diffraction peak centered at  $2\theta = 25^\circ$  was observed for PANI, and this peak was overwhelmed by the strong diffraction peaks of Fe<sub>3</sub>O<sub>4</sub> in the FP materials. This indicates that the PANI layer had formed on the surface of the Fe<sub>3</sub>O<sub>4</sub> nanoparticles.

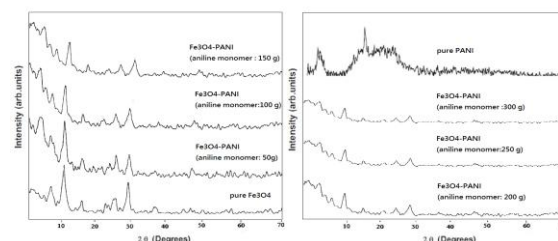


**Fig. 3:** The XRD patterns associated with the various added aniline monomer

The SEM results further confirm the successful polymerization of aniline onto the Fe<sub>3</sub>O<sub>4</sub> core (Fig. 4a). The PANI particles and aggregation in the FP samples could not be found in the SEM images. The observation indicated that PANI was uniformly coated on the Fe<sub>3</sub>O<sub>4</sub> nanoparticles during the

polymerization process. In addition, Fig. 4 shows the hollow PANI spheres, which were obtained by etching the  $\text{Fe}_3\text{O}_4$  templates with HF solution. It can be seen that although  $\text{Fe}_3\text{O}_4$  particles had been removed, the structural of the PANI sphere was still maintained after the etch reaction in acidic condition. This means that  $\text{Fe}_3\text{O}_4$  nanoparticle acts a template for the deposition of PANI during the reaction. The PANI thickness is linearly proportional to the weight of aniline. These results mean that the double-surfactant assist polymerization method can appropriately control the fabrication of the PANI shell on the surface of the  $\text{Fe}_3\text{O}_4$  core.

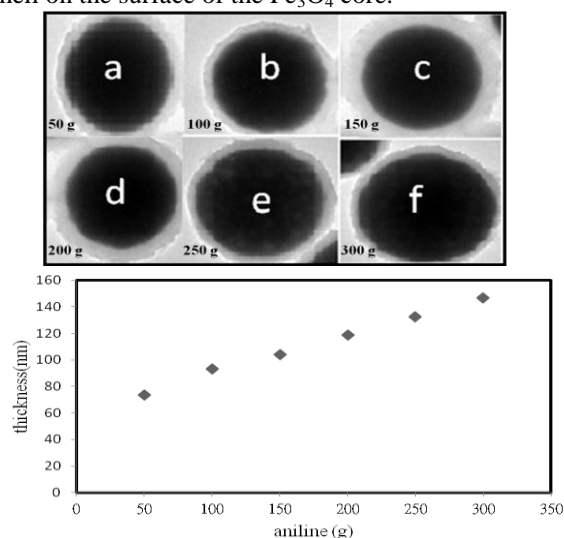


**Fig. 4:** (a) Scanning electron microscope image and (b) PANI thickness with the added aniline monomer

The forming mechanism of the PANI shell uniformly coated on the  $\text{Fe}_3\text{O}_4$  core is proposed as follows. In the double-surfactant polymerization, PEG and DBSA act as surfactants. Adding PVP can improve the dispersibility of the  $\text{Fe}_3\text{O}_4$  nanoparticles in aqueous solution. Before the polymerization reaction, DBSA was added to the PEG-adsorbed  $\text{TiO}_2$  solution. DBSA could dissociate into dodecyl benzene sulfonic (DBS) ions and a double-surfactant layer (PEG-DBS layer), which was expected to form with polar amide groups of PEG surrounded on the surface of the  $\text{Fe}_3\text{O}_4$  core and the negative side of DBS molecule facing out to the solution. Subsequently, aniline monomers were added and converted into cationic anilinium ions under an acidic condition. The cationic anilinium ions were adsorbed on the surface of the negatively charged  $\text{Fe}_3\text{O}_4$  core because of electrostatic forces. The adsorption engendered a considerable increase in the local concentration of aniline monomers near the core surface. This consequently initiated the polymerization of aniline at low concentration of aniline monomers. Therefore, the polymerization was initiated, propagated, and terminated on the surface of the  $\text{Fe}_3\text{O}_4$  core rather than in solution. A

homogeneous, continuous, and uniform PANI shell was eventually formed on the surface of the  $\text{Fe}_3\text{O}_4$  core.

According to the experimental data presented in Table 2, the PANI sample with weight of aniline monomer reached 50 g exhibited a special surface area ( $S_{\text{BET}}$ ) of  $1030 \text{ m}^2/\text{g}$ , mean pore size of 6.4 nm and porosity of 75.4 %. The  $S_{\text{BET}}$  is evidently higher than previously reported value [29], which can be attributed to the reduced aggregation states of the  $\text{Fe}_3\text{O}_4$  nanoparticles and the highly porous structure induced by the freeze-drying process of the synthesis of the core-shell nanocomposites [23]. In addition, the data of the materials slowly increases until the weight value reached 250 g, and subsequently, the data decreased as the weight value increased to 300 g. The performance can be explained by the pore formation of a freeze-dried polymer. Studies have reported that the freeze-drying technique is based on sublimation [26]. The material to be dried is frozen quickly at a low temperature and then dried in a vacuum. The solvent molecules directly sublimate and escape as vapors, and porous structures are formed from the voids created by the removal of the solvent. Finally, a polymer porous film with an interpenetrating network structure can be obtained. When the PANI content is excessively low, the PANI shell structure demonstrates larger pores, preventing it from forming a stable porous surface. By contrast, when the PANI content is excessively high, maintaining satisfactory fluidity is difficult, affecting the growth of solvent crystals. The theory was confirmed with the SEM results. When the aniline monomers were 50 g, the PANI shell demonstrated a nonuniform mesh-like structure (Fig. 5a); when the aniline monomers were 100–200 g, the shell exhibited a lamellar structure (Figs. 5b–5d). Moreover, when the aniline monomers were 250 g, the PANI shell demonstrated a lamellar structure, with nonuniform pores occurring between the polymer layers (Fig. 5e). In addition, when the aniline monomers were 300 g, the PANI shell exhibited lamellar polymer layers arranged in various orientations (Fig. 5f).

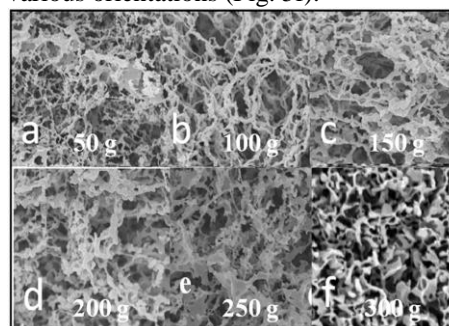


**Fig. 5:** Surface structure characterization with the added aniline monomer

**TABLE 2: Physical characterization with the added aniline monomer**

Aniline monomer (g)	Shell thickness (nm)	S <sub>BET</sub> (m <sup>2</sup> /g)	Mean pore size (nm)	Porosity (%)
50	130	1030	6.4	75.4
100	165	1131	7.5	78.6
150	184	1236	8.8	83.1
200	210	1442	10.8	86.5
250	235	1452	12.9	87.4
300	260	654	6.5	55.4

4.2 DC Conductivity

Table 3 shows the variation in DC conductivity as a function of the temperature and PANI thickness. The conductivities remained unchanged until the temperature was up to 50°C, and they proportionally increased as the temperature increased from 50 to 125°C. Moreover, the conductivities decreased when the temperature increased up to 200°C. This phenomenon can be explained as follows. In the amorphous phase of the CPs, each atom contains a certain number of electrons and is electrically neutral [33,34]. At low temperatures, an electron requires a certain amount of activation energy to move away from a site. Insufficient energy engenders failure in the formation of charged defects [35]. However, sufficient energy increases the charge propagation along one-dimensional conjugated domains with cross-conjugation defects at the tunneling junction. The reduction in the conductivities can be attributed to the occurrence of a thermally activated barrier. The bonding in the conjugated backbone of the CP is not highly strong; therefore, as the thermal energy exceeds a critical value, the thermal vibrations of PANI contribute to an increase in electrical resistance, consequently degrading the skeletal PANI chain structure [36]. At the characteristic temperature of 125°C, the conductivity gradually increased until the amount of aniline was up to 250 g. Moreover, when the amount of aniline increased to 300 g, the conductivity clearly decreased. The result is similar to the distribution of the specific surface area presented in Table 2. A larger specific surface area leads to more electrochemically active sites and longer conjugation length [37], and this is useful in the formation of a complete charge-transfer network in the PANI chains, providing a more favorable path for electron delocalization.

**TABLE 3: DC conductivity (10<sup>-2</sup> s/cm) on exposure for various operating temperatures**

PANI thickness (nm)	Reaction temperature							
	25 °C	50 °C	75 °C	100 °C	125 °C	150 °C	175 °C	200 °C
130	0.2	0.25	0.48	0.96	1.92	1.81	0.22	0
165	0.2	0.28	0.76	1.56	3.64	3.5	0.24	0
184	0.2	0.36	1.45	2.69	5.74	3.54	0.31	0
210	0.2	0.49	3.85	5.55	7.16	3.24	0.42	0
235	0.2	0.52	6.86	8.12	13.65	0.49	0.28	0
260	0.2	0.22	0.35	1.42	3.48	0.15	0.19	0

130	0.2	0.25	0.48	0.96	1.92	1.81	0.22	0
165	0.2	0.28	0.76	1.56	3.64	3.5	0.24	0
184	0.2	0.36	1.45	2.69	5.74	3.54	0.31	0
210	0.2	0.49	3.85	5.55	7.16	3.24	0.42	0
235	0.2	0.52	6.86	8.12	13.65	0.49	0.28	0
260	0.2	0.22	0.35	1.42	3.48	0.15	0.19	0

4.3 Detection of OH Radicals

Fig. 6 shows that the OH radical yield increased linearly with the amount of ozone consumed. When the ozone consumption was 10–100 ppm, α-FeOOH generated 1.8×10<sup>8</sup> to 9.75 ×10<sup>8</sup> radicals/cm<sup>3</sup>, yielding an average OH-radical-to-ozone molar ratio of 0.29–0.31. The yield rate of OH radicals generated through catalytic ozonation was a second-order kinetic relative to the ozone and OH group concentrations on the surface of the catalyst. When the OH group was fixed, the generation of OH radicals on the catalyst surface was proportional to the ozone consumed. At the characteristic temperature of 125°C, the Δσ values of the PANI sample with the highest SBET were exponentially proportional to the OH radicals produced from the consumption of ozone. The result showed high Δσ values for more than 5% change in the concentration of OH radicals from 5.23 × 10<sup>8</sup> to 11.3 × 10<sup>8</sup> radicals/cm<sup>3</sup>. The results reveal that the high amount of OH radicals in air positively influenced the drop in conductivity in the PANI sample. The conductivity of PANI can be reduced through an oxidative doping process by using strong oxidants. Gas-phase OH radicals are one of the strongest and most sensitive oxidants. Therefore, when the PANI composite was exposed to air containing OH radicals, the insufficient OH radicals were easily self-decomposed across the OH radical–PANI chain collision interface. The sufficient OH radicals diffused into the surface of the PANI shell, the adsorbed OH radicals inserted anionic species in the PANI backbone structure, leading to the formation of a material exclusively displaying the property of anionic species [38,39]. Consequently, a decrease in the electrical conductivity of the PANI composite was associated with a reversible strong oxidation by the OH radicals [40].

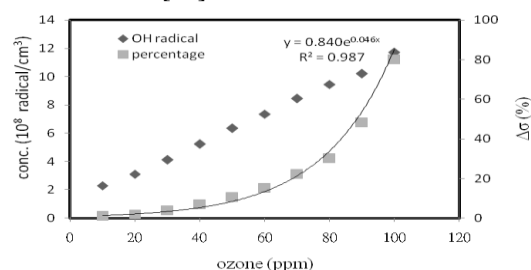


**Fig. 6:** Conductivity recorded after the OH radical attack by adjusting the ozone consumed.

## V. CONCLUSIONS

In summary, Fe<sub>3</sub>O<sub>4</sub> nanoparticles were used as a template to produce hollow PANI spheres through a double-surfactant-layer-assisted-polymerization process. The surface structure and shell thickness could be effectively controlled by modulating the added aniline monomers. The implemented electronic OH radical sensors were fabricated by coating hollow PANI capsules on a Si<sub>3</sub>N<sub>4</sub>/Si substrate with deposited gold metal electrodes. At the characteristic activation temperature of 125 °C, the conductivities engendered an increase in sensitivity for the PANI composite with increasing S<sub>BET</sub>. Among all composites, the PANI sensor with a characteristic S<sub>BET</sub> of 1452 m<sup>2</sup>/g exhibited the highest conductivity. The conductometric behavior induced by the OH radical attack was exponentially proportional to the concentration of OH radicals. Hence, we suggest that hollow PANI spheres are a promising material for high-performance gas-phase OH radical sensing applications.

## REFERENCES

- [1]. E. Sahle-Demessie and V.G. Devulapelli, Vapor phase oxidation of dimethyl sulfide with ozone over V<sub>2</sub>O<sub>5</sub>/TiO<sub>2</sub> catalyst, *Applied Catalysis B: Environmental*, 84(3-4), 2008, 408-419.
- [2]. A.A. Bakheet, M.F. Mohd Zain, A.A. Kadhum, and Z. Abdalla, Photocatalytic oxidation performance to removal of volatile organic compounds in indoor environment, *Environmental Research, Engineering and Management*, 4(58), 2011, 27-33.
- [3]. C. Subrahmanyam, Catalytic non-thermal plasma reactor for total oxidation of volatile organic compounds, *Indian Journal of Chemistry*, 48(A), 2009, 1062-1068.
- [4]. S.K. Han, S.N. Nam, J.W. Kang, OH radical monitoring technologies for AOP advanced oxidation process. *Water Science and Technology*, 46(11-12), 2002, 7-12.
- [5]. E.J. Rosenfeldt, K.G. Linden, S. Canonica, and U. von Gunten, Comparison of the efficiency of \*OH radical formation during ozonation and the advanced oxidation processes O<sub>3</sub>/H<sub>2</sub>O<sub>2</sub> and UV/H<sub>2</sub>O<sub>2</sub>, *Water Research*, 40(20), 2006, 3695-3704.
- [6]. P. Attri, Y.H. Kim, D.H. Park, J.H. Park, Y.J. Hong, H.S. Uhm, K.N. Kim, A. Fridman, and E.H. Cho, Generation mechanism of hydroxyl radical species and its lifetime prediction during the plasma-initiated ultraviolet (UV) photolysis, *Scientific Reports*, 5(9332), 2015.
- [7]. M.W. Teague, T. Felix, M.K. Hudson, and R. Shanks, Application of hydroxyl (OH) radical ultraviolet absorption spectroscopy to rocket plumes, *Journal of Pyrotechnics*, 16, 2002, 71-75.
- [8]. H.U. Stauffer, J.R. Gord, W.D. Kulatilaka, and S. Roy, Laser-induced fluorescence detection of hydroxyl (OH) radical by femtosecond excitation, *Optics Letters*, 36(10), 2011, 1776-1778.
- [9]. B. Liu and H.X. Wang, Determination of atmospheric hydroxyl radical by HPLC coupled with electrochemical detection, *Journal of Environmental Sciences*, 20(1), 2008, 28-32.
- [10]. S. Wang, L. Hu, Y. Hu, and S. Jiao, Conductive polyaniline capped Fe<sub>2</sub>O<sub>3</sub> composite anode for high rate lithium ion batteries, *Materials Chemistry and Physics*, 146, 2014, e289-e294.
- [11]. H. Shirakawa, E.J. Louis, A.G. MacDiarmid, C.K. Chiang, and A.J. Heeger, Synthesis of electrically conducting organic polymers: halogen derivatives of polyacetylene, (CH)<sub>x</sub>, *Journal of the Chemical Society, Chemical Communications*, 16, 1977, 578-580.
- [12]. D.D. Ateh, H.A. Navsaria, and P. Vadgama, Polypyrrole-based conducting polymers and interactions with biological tissues, *Journal of the Royal Society Interface*, 3(11), 2006, 741-752.
- [13]. X.Y. Zhao and M.Z. Wang, Structure dependence of photochromism and thermochromism of azobenzene-functionalized polythiophenes, *EXPRESS Polymer Letters*, 1(7), 2007, 450-455.
- [14]. I. Rodríguez, B.R. Scharifker, and J. Mostany, In situ FTIR study of redox and overoxidation processes in polypyrrole films, *Journal of Electroanalytical Chemistry*, 491, 2000, 117-125.
- [15]. A. Parsa, M. Sadeghi, M. Maleki, S. Parhizkar, and S. Ab Ghani, Free radical scavenging activity of homo and copolymer of aniline and para-phenylenediamine prepared in ZnCl<sub>2</sub> medium, *Electrochimica Acta*, 127, 2014, 34-38.
- [16]. M. Gizdavic-Nikolaidis, J. Travas-Sejdic, G.A. Bowmaker, R.P. Cooney, and P.A. Kilmartin. Conducting polymers as free radical scavengers, *Synthetic Metals*, 140(2-3), 2004, 225-232.
- [17]. L. Wu, Y.X. Zhang, and C.S. Zhang, Research of in situ polymerization and core-shell structure modified emulsified asphalt, *Applied Mechanics and Materials*, 71-78, 2011, 928-931.

- [18]. G. Li, C. Zhang, H. Peng, and K. Chen, One-dimensional  $V_2O_5@$  polyaniline core/shell nanobelts synthesized by an in situ polymerization method, *Macromolecular Rapid Communications*, 30(21), 2009, 1841-1845.
- [19]. A.M. Keene and K.M. Tyner, Analytical characterization of gold nanoparticle primary particles, aggregates, agglomerates, and agglomerated aggregates, *Journal of Nanoparticle Research*, 13(8), 2011, 3465-3481.
- [20]. R. Hayes, A. Ahmed, T. Edge, and H. Zhang, Core-shell particles: Preparation, fundamentals and applications in high performance liquid chromatography, *Journal of Chromatography A*, 1357, 2014, 36-52.
- [21]. M.J. Smith, V.H.B. Ho, N.J. Darton, and N.K.H. Slater, Effect of magnetite nanoparticle agglomerates on ultrasound induced inertial cavitation, *Ultrasound in Medicine & Biology*, 35(6), 2009, 1010-1014.
- [22]. J.A. Siriviriyannun, E.A. O'Rear, and N. Yanumet, Modification of polyester fabric properties by surfactant-aided surface polymerization, *Journal of Applied Polymer Science*, 103(6), 2007, 4059-4064.
- [23]. S. Samitsu, R. Zhang, X. Peng, M.R. Krishnan, Y. Fujii, and I. Ichinose, Flash freezing route to mesoporous polymer nanofibre networks, *Nature Communications*, 4(2653), 2013.
- [24]. B. Lin and S.L. Liaw, Simultaneous removal of volatile organic compounds from cooking oil fumes by using gas-phase ozonation over  $Fe(OH)_3$  nanoparticles, *Journal of Environmental Chemical Engineering*, 3(3), 2015, 1530-1538.
- [25]. X. Xu and S.A. Asher, Synthesis and utilization of monodisperse hollow polymeric particles in photonic crystals, *Journal of the American Chemical Society*, 126(25), 2004, 7940-7945.
- [26]. K. Robbie and M.J. Brett, Sculptured thin films and glancing angle deposition: Growth mechanics and applications, *Journal of Vacuum Science & Technology A*, 15(3), 1997, 1460-1465.
- [27]. I. Bull, W.M. Xue, P. Burk, R.S. Boorse, W.M. Jaglowski, G.S. Koermer, A. Moini, J.A. Patchett, J.C. Dettling, and M.T. Caudle, Copper CHA zeolite catalysts, U.S. Patent 7601662, 2009.
- [28]. J.D.F. Ramsay and B.O. Booth, Neutron scattering and adsorption isotherm studies of structure in oxide sols and gels, *Studies in Surface Science and Catalysis*, 10, 1982, 211-225.
- [29]. L. Diez, M.H. Livertoux, A.A. Stark, M. Wellman-Rousseau, and P. Leroy, High-performance liquid chromatographic assay of hydroxyl free radical using salicylic acid hydroxylation during in vitro experiments involving thiols, *Journal of Chromatography B: Biomedical Sciences and Applications*, 763(1), 2001, 185-193.
- [30]. S.C. Nagaraju, A.S. Roy, and J.B.P. Kumar, Humidity sensing properties of surface modified polyaniline metal oxide composites, *Journal of Engineering*, Article ID 925020, 2014, 8 pages.
- [31]. W. Cheng, K. Tang, Y. Qi, J. Sheng, and Z. Liu, One-step synthesis of superparamagnetic monodisperse porous  $Fe_3O_4$  hollow and core-shell spheres, *Journal of Materials Chemistry*, 20(9), 2010, 1799-1805.
- [32]. Y. Yang and J.S. Jiang, Gradual phase and morphology transformation of  $Fe_3O_4$  nanoparticles to  $\alpha$ - $FeOOH$  nanorods in alcohol/water media in the presence of surfactant F127, *Journal of Materials Science*, 43(12), 2008, 4340-4343.
- [33]. J.E. Hout, D. Chatain, C. Lacabann, A. Montanerb, and M. Galtierb, Characterization of the amorphous phase of polyacetylene by thermally stimulated currents, *Macromolecular Symposia*, 24(1), 1989, 129-136.
- [34]. J.R. Araujo, C.B. Adamob, E. De Robertisa, A.Y. Kuznetsova, B.S. Archanjoa, B. Fragneauda, C.A. Achetea, and M-A. De Paoli, Crystallinity, oxidation states and morphology of polyaniline coated curauá fibers in polyamide-6 composites, *Composites Science and Technology*, 88, 2013, 106-112.
- [35]. A.S. Zakirov, K.T. Igamberdiev, A.T. Mamadalimov, L.F. Musaeva, and A.A. Saidov, Influence of structural defects on the thermophysical and magnetic properties of polyaniline, *Journal of Engineering Physics and Thermophysics*, 76(5), 2003, 1089-1092.
- [36]. O. Misoon and K. Seok, Effect of dodecyl benzene sulfonic acid on the preparation of polyaniline/activated carbon composites by in situ emulsion polymerization, *Electrochimica Acta*, 59 (1), 2012, 196-201.
- [37]. M.J. Watt-Smith, J.M. Friedrich, S.P. Rigby, T.R. Ralph, and F.C. Walsh, Determination of the electrochemically active surface area of Pt/C PEM fuel cell

- electrodes using different adsorbates, *Journal of Physics D: Applied Physics*, 41(17), 2008, article id. 174004.
- [38]. X. Zhang, E.T. Kang, K.G. Neoh, K.L. Tan, D.Y. Kim, and C.Y. Kim. Surface studies of pristine and surface-modified polypyrrole films, *Journal of Applied Polymer Science*, 60(4), 1996, 625-636.
- [39]. O. Inganas, R. Erlandson, C. Nylander, and I. Lundstrom, Proton modification of conducting polypyrrole, *Journal of Physics Chemistry of Solids*, 45(4), 1984, 427-432.
- [40]. C. Debiemme-Chouvy and T.T.T.M. Tren, An insight into the overoxidation of polypyrrole materials, *Electrochemistry Communications*, 10(6), 2008, 947-950.